Journal of Power Sources 214 (2012) 195–199

Contents lists available at SciVerse ScienceDirect

Journal of Power Sources

journal homepage: www.elsevier.com/locate/jpowsour

Short communication

Nano-$Li_4Ti_5O_{12}$ anchored on carbon nanotubes by liquid phase deposition as anode material for high rate lithium-ion batteries

Haifang Ni, Li-Zhen Fan*

School of Materials Science and Engineering, University of Science and Technology Beijing, Beijing 100083, China

HIGHLIGHTS

- We report a liquid phase deposition to synthesize nano-$Li_4Ti_5O_{12}$ anchored on CNTs.
- The obtained $Li_4Ti_5O_{12}$ are 10–30 nm in size on CNTs surface.
- Nano-$Li_4Ti_5O_{12}$/CNTs composite can decrease the polarization of electrode.
- This nano-$Li_4Ti_5O_{12}$/CNTs composite displays superior electrochemical performance.

ARTICLE INFO

Article history:
Received 19 January 2012
Received in revised form
26 March 2012
Accepted 25 April 2012
Available online 4 May 2012

Keywords:
Lithium ion batteries
Lithium titanate
Carbon nanotubes
Nanocomposite
Anode materials

ABSTRACT

Functionalized multi-walled carbon nanotubes (CNTs) are homogeneously anchored with ~50 nm in size of Lithium titanate ($Li_4Ti_5O_{12}$) by the controlled hydrolysis of tetrabutyl titanate. The resulted $Li_4Ti_5O_{12}$/CNT composite has been investigated for electrochemical activity with lithium ion batteries, displaying high-rate capacity of 112 mAh g^{-1} at 20 C. Furthermore, the composite exhibits good cycle stability, retaining over 98% of its initial capacity after 100 cycles at 5 C. The high capacity is attributed to the unique property of the $Li_4Ti_5O_{12}$/CNTs nanocomposite, which provides a short diffusion path for lithium ions and rapid conducting for charge carrier through the high conductivity of CNTs network.

1. Introduction

The spinel $Li_4Ti_5O_{12}$ has been emerging as one promising next generation's anode material for high power lithium ion batteries as well as hybrid supercapacitors, owing to its inherent characteristics [1–5]. Compared to carbon based anode materials, the spinel $Li_4Ti_5O_{12}$ shows a higher redox potential of approximately 1.55 V (vs. Li/Li^+), which can avoid the reduction of the electrolyte on the electrode surface and the formation of a solid electrolyte interface [6–8]. Furthermore, as a zero-strain insertion material, the spinel $Li_4Ti_5O_{12}$ possesses excellent reversibility, structural stability and excellent lithium ion mobility in the charge–discharge process, which makes $Li_4Ti_5O_{12}$ particularly attractive for large scale energy storage [9,10]. However, $Li_4Ti_5O_{12}$ is insulating in nature with a low electronic conductivity ($<10^{-9}$ S m^{-1}), resulting in poor rate capability and the great degradation of capacity upon prolonged cycling [11]. Many efforts have been taken to ameliorate its rate capability, including tailoring particle size [12,13] and surface coatings with conductive materials [14–16] or doping the other metal ions [17–20]. Recently, nanostructured $Li_4Ti_5O_{12}$ is expected to exhibit ameliorated rate capability because of the short transport path of lithium ions and electrons. Also, the nanostructure offers sufficient contact interface between active materials and electrolyte, resulting in a high Li storage capacity and high rates of insertion.

Carbon nanotube is a one-dimensional tubular structure nanomaterial, which is considered to be an excellent substrate to host active nanomaterials for energy applications due to its superior electrical conductivity, large surface area, chemical and mechanical stability [21–24]. Numerous CNTs-based inorganic nanocomposite with metal and metal oxides have been successfully synthesized, showing excellent properties of these host materials [25–28]. It is well accepted that nanomaterials have potential advantages of good cycling performance and short path for Li^+ transport over

* Corresponding author. Tel./fax: +86 10 62334311.
E-mail address: fanlizhen@ustb.edu.cn (L.-Z. Fan).

0378-7753/$ – see front matter © 2012 Elsevier B.V. All rights reserved.
doi:10.1016/j.jpowsour.2012.04.074

their bulk counterparts due to the large contact area between electrode and electrolyte [29,30]. Therefore, it is highly desirable to improve the capacity of $Li_4Ti_5O_{12}$ by electrically wiring up $Li_4Ti_5O_{12}$ nanoparticles to an underlying conducting CNTs substrate. Among many reported methods for this binary composite, sol–gel method, followed by heat-treatment at elevated temperatures, is the most common method to introduce the inorganic phase onto the CNTs substrate. Despite the remarkable progress, many technical issues related to the sol–gel method remain to be addressed [31–34]. For instance, the heat-treatment process often causes the phase separation between surface $Li_4Ti_5O_{12}$ and underneath CNTs, leading to unwanted particles growth.

Here, we report a facile liquid phase deposition method to synthesize composite of $Li_4Ti_5O_{12}$ nanoparticles anchored on conducting CNTs substrate as an anode material. The obtained $Li_4Ti_5O_{12}$ nanoparticles are about 50 nm in size and homogeneously anchored on the surface of CNTs. The nano-$Li_4Ti_5O_{12}$/CNTs composite exhibited superior performance with high reversible capacity, excellent cyclic performance and good rate capability.

2. Experimental

All of the reactants were of analytical grade and used without further purification. The multi-walled CNTs with an outer diameter of about 40–60 nm were purchased from Shenzhen Nanotech Port Co. Ltd. The pristine CNTs were purified by ultrasonic treatment in 2.6 mol L^{-1} nitric acid for 0.5 h, and washed by deionized water and ethanol, then drying for 12 h under vacuum at 80 °C before use.

The nano-$Li_4Ti_5O_{12}$/CNTs composite was prepared by a liquid phase deposition method. The predetermined amount of CNT in nano-$Li_4Ti_5O_{12}$/CNTs composite is 10 wt%. Typically, 0.3 g purified CNTs were dispersed in 24 mL ethanol with sonication for 1 h and then 10.2 g tetrabutyl titanate was added under vigorous magnetic stirring. 1.6632 g lithium acetate was dissolved into 26 mL of ethanol–water mixture (12:1 in volume) and slowly dropped into the above suspension. After 24 h continuous stirring, the mixture was aged at 60 °C over 60 h to remove solvents gradually and ground in a mortar. The precursor was calcined at 900 °C under N_2 for 1 h with a heating rate of 5 °C min^{-1} to obtain the nano-$Li_4Ti_5O_{12}$/CNTs composite.

For comparison, the bulk $Li_4Ti_5O_{12}$/CNTs composite was prepared via a sol–gel route using acetic acid as the chelating agent. In a typical procedure, 0.3 g purified CNTs and 4 mL acetic acid were dispersed in 24 mL ethanol with sonication for 1 h and then 10.2 g tetrabutyl titanate and 2 mL hydrochloric acid were added under vigorous stirring to obtain the solution A. 1.6632 g lithium acetate was dissolved in the mixture solutions of 12 mL ethanol and 2 mL deionize water to obtain solution B. With stirring, B solution was gradually dropped into A solution and then a colloidal solution was obtained. After slowly hydrolyzing for several hours, gel formed. The resulting gel was dried at 60 °C over 60 h to extract out excess solvents and yield dried gel precursors. The dried gel was preheated at 450 °C for 5 h and then calcined at 800 °C for 10 h to obtain the bulk $Li_4Ti_5O_{12}$/CNTs composite.

The crystal structure of the as-prepared materials were characterized by X-ray diffraction measurements (XRD, Rigaku/mac250) using Cu Kα radiation in the 2θ range of 10–90°. The microstructural of the synthesized materials were observed by field-emission scanning electron microscopy (FESEM, ZEISS supra 55) and transmission electron microscopy (TEM, JEOL JEM-200CX). Thermogravimetric (TG) analysis was performed on a TG instrument (Mettler-Toledo TGA/DSC 1) with a heating rate of 5 °C min^{-1} from 50 to 800 °C in air atmosphere.

The electrochemical properties were carried out by galvanostatic cycling in a two-electrode electrochemical cell. The working electrodes were prepared by mixing 80 wt.% active materials, 10 wt.% Super P, and 10 wt.% polyvinylidene fluoride dissolved in N-methylpyrrolidinone. The resultant slurry, spread uniformly on copper foil, was dried at 120 °C under vacuum for 12 h. The coin cells (2032) were assembled in an argon-filled glove box using Li foil as counter electrode, Celgard 2400 as separator, and 1 M $LiPF_6$ in a 1:1:1 (volume) mixture of ethylene carbonate, dimethyl carbonate and ethylmethyl carbonate as the electrolyte. The cells were tested at various current densities using a LAND-CT2001A cell test instrument with voltage window of 1–2.5 V (vs. Li/Li^+). Cyclic voltammograms were recorded from 1 to 2.5 V at different scanning rates using a CHI660C electrochemical workstation.

3. Results and discussion

As mentioned above, our synthesis process is different from the previously reported preparation of $Li_4Ti_5O_{12}$/CNTs composites [35–37], in which nanoparticles were mechanically mixed with CNTs. The overall synthetic process of $Li_4Ti_5O_{12}$/CNTs nanocomposite is illustrated in Fig. 1. Firstly, the CNTs surfaces was functionalized using concentrated nitric acid that introduces functional groups such as carboxyl (–COOH), hydroxyl (–OH), and carbonyl (–CO) groups. These functional groups not only facilitate the dispersion of CNTs but also serve as nucleation centers for the condensation and polymerization. Then, the TiO_2 nanoparticles were anchored on the surface of CNTs by the controlled hydrolysis of tetrabutyl titanate. Finally, the TiO_2/CNTs were converted to $Li_4Ti_5O_{12}$/CNTs nanocomposite by a short heat-annealing.

Fig. 2 presents the XRD patterns of the CNTs, bulk $Li_4Ti_5O_{12}$/CNTs and nano-$Li_4Ti_5O_{12}$/CNTs composites. The CNTs displays a broad diffraction peak centered at $2\theta = 26°$, which corresponds to the (002) plane of the stacked graphene layers in the CNTs. The main diffraction peaks of bulk $Li_4Ti_5O_{12}$/CNTs and nano-$Li_4Ti_5O_{12}$/CNTs can be indexed as a cubic spinel structure $Li_4Ti_5O_{12}$ according to JCPDS No.00-49-0207 and no impurity peaks can be found.

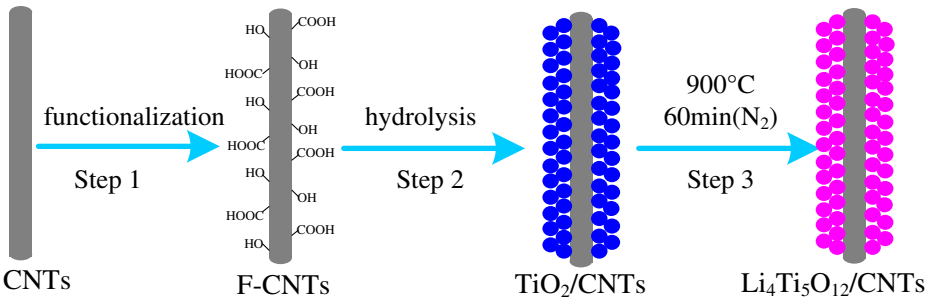

Fig. 1. Schematic illustration of the synthesis process of nano-$Li_4Ti_5O_{12}$/CNTs composite by a liquid phase deposition.

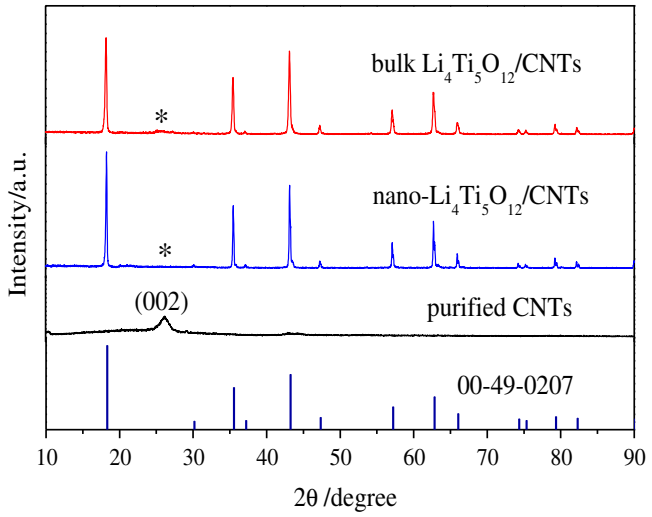

Fig. 2. XRD patterns of purified CNTs, bulk $Li_4Ti_5O_{12}$/CNTs composite and nano-$Li_4Ti_5O_{12}$/CNTs composites.

Furthermore, an additional small and low broad diffraction peak labeled by asterisk (*) appears at 2θ value of 26°, which corresponds to the typical diffraction peaks of CNTs. These results indicate that the addition of CNTs has no influence on the crystal structure of spinel $Li_4Ti_5O_{12}$ during the heat-treatment.

Fig. 3 displays the FESEM and TEM images of the purified CNTs, nano-$Li_4Ti_5O_{12}$/CNTs, and bulk $Li_4Ti_5O_{12}$/CNTs respectively. Fig. 3a presents the image of the randomly entangled CNTs with an outer diameter of approximately 40–60 nm. From the image of the nano-$Li_4Ti_5O_{12}$/CNTs composite (Fig. 3b), it can be seen that the $Li_4Ti_5O_{12}$ nanoparticles have a size of ~50 nm and are homogeneously anchored on the surface of functionalized CNTs, and the CNTs extends in all directions like a stretched network. It should be emphasized that the crystal structure and grain size of bulk $Li_4Ti_5O_{12}$/CNTs composite obtained by sol–gel method have been changed obviously. The size of $Li_4Ti_5O_{12}$ particles in $Li_4Ti_5O_{12}$/CNTs composite is about 200–700 nm and some of them aggregated (Fig. 3c). The functionalized CNTs are distributed among $Li_4Ti_5O_{12}$ particles randomly. TEM was further performed to characterize the microstructures and crystal structures of the nano-$Li_4Ti_5O_{12}$/CNTs composite (Fig. 3d). It is clear that a very large quantity of the $Li_4Ti_5O_{12}$ nanoparticles with a size of ~50 nm were uniformly anchored on the surface of CNTs. As can be seen from Fig. 3d inset, there are two kinds of lattice fringes with a lattice spacing of about 0.48 nm and 0.34 nm corresponding to the (111) plane of spinel $Li_4Ti_5O_{12}$ and the (002) crystalline planes of the multi-walled CNTs respectively, which confirms the formation of the nano-$Li_4Ti_5O_{12}$/CNTs composite. Additionally, no obvious aggregations of the $Li_4Ti_5O_{12}$ nanoparticles are observed in the composite, indicating that the nuclei are predominantly on the exterior surfaces of CNTs. Although the exact growth mechanism has not been completely understood, we suggest that oxygen containing functional groups on functionalized CNTs can act as anchoring or nuclei for the growth of $Li_4Ti_5O_{12}$. During the calcination process, many nuclei form on the surface of CNTs and grow in the same time, resulting in smaller size of $Li_4Ti_5O_{12}$ particles. It is worth noting that during the calcination process, the nanoparticles are still strongly anchored on the surface of CNTs with a high density, suggesting a strong interaction between nanoparticles and CNTs. The strong anchoring of $Li_4Ti_5O_{12}$ nanoparticles on CNTs surface enables fast electron transport through the underlying CNTs to nanoparticles, resulting in superior rate capability. On the other hand, the nanoparticles anchored on the surface of CNTs can act as spacers to efficiently

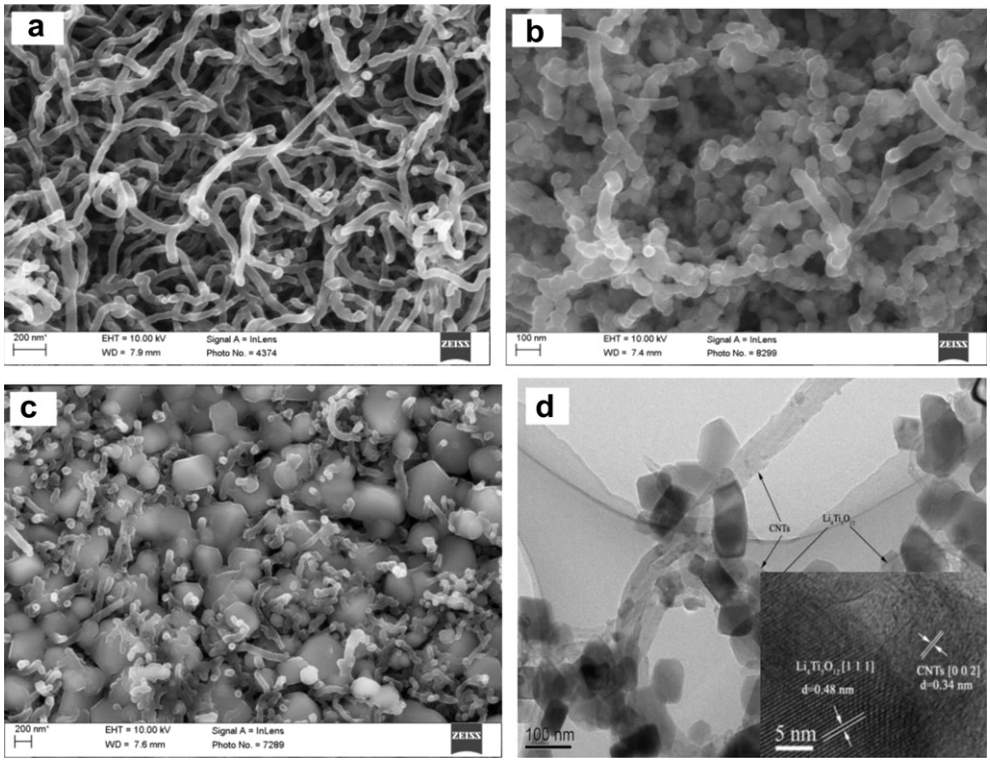

Fig. 3. FESEM images of functionalized CNTs (a), nano-$Li_4Ti_5O_{12}$/CNTs composite synthesized by liquid phase deposition (b), and bulk $Li_4Ti_5O_{12}$/CNTs composite synthesized by sol–gel method (c); TEM image (d) and high resolution TEM image (inset of d) of nano-$Li_4Ti_5O_{12}$/CNTs composite synthesized by liquid phase deposition.

prevent the restacking of CNTs, weakening the loss of their high active surface area. The TG result indicates that the exact content of CNTs in the nano-$Li_4Ti_5O_{12}$/CNTs composite was 9.64 wt.% (Fig. 4), which is quite close to the predetermined ratio.

The electrochemical performance of the nano-$Li_4Ti_5O_{12}$/CNTs electrodes was characterized by cyclic voltammograms (CV) within a potential window of 1–2.5 V (vs. Li/Li^+). From the CV comparison shown in Fig. 5, it can be seen that the CV curve of the nano-$Li_4Ti_5O_{12}$/CNTs electrode is similar to that of the bulk $Li_4Ti_5O_{12}$/CNTs electrode and a pair of reversible redox peaks can be clearly observed. In addition, the anodic and cathodic peaks are sharp, indicating the good electrode kinetic process of the nano-$Li_4Ti_5O_{12}$/CNTs composite. At a scan rate of 1 mV s^{-1}, it should be noted that the redox peak profile is located at 1.460/1.736 V (vs. Li/Li^+) for the nano-$Li_4Ti_5O_{12}$/CNTs composite, and 1.372/1.781 V for the bulk $Li_4Ti_5O_{12}$/CNTs. The potential separation between the oxidation and reduction peaks can reflect the polarization degree of the electrode. The nano-$Li_4Ti_5O_{12}$/CNTs electrode has a smaller potential separation compared with the bulk $Li_4Ti_5O_{12}$/CNTs electrode, showing a weak polarization. These could be attributed to the following reason. First, the smaller size (~50 nm) makes shorter distance for Li^+ ions diffusion in $Li_4Ti_5O_{12}$ particles, and benefits the diffusion process. Moreover, the higher surface area of nano-$Li_4Ti_5O_{12}$/CNTs composite providing a higher electrode/electrolyte contact surface area results in the low current density and low electrochemical reaction resistance during the rapid charge/discharge process.

The discharge curves of the nano-$Li_4Ti_5O_{12}$/CNTs and bulk $Li_4Ti_5O_{12}$/CNTs electrodes at different rates are shown in Fig. 6. For the nano-$Li_4Ti_5O_{12}$/CNTs (Fig. 6a), the discharge capacity is 171 mAh g^{-1} at 1 C (the capacity is calculated based on the weight of the $Li_4Ti_5O_{12}$ in the $Li_4Ti_5O_{12}$/CNTs electrode. If the weights of CNTs are included, the overall capacities of the composites should be ~90% of the reported capacities.), very close to the theoretical value (175 mAh g^{-1}), while it is only 162.9 mAh g^{-1} for the bulk $Li_4Ti_5O_{12}$/CNTs (Fig. 6b). Although the cell voltage decreases with increasing current density, it also shows a flat potential plateau even at 20 C. At the rate of 10 C, the bulk $Li_4Ti_5O_{12}$/CNTs has no clear discharge voltage plateau, and the capacity is only 76.4 mAh g^{-1}. Fig. 7 compares the rate capabilities of the nano-$Li_4Ti_5O_{12}$/CNTs and bulk $Li_4Ti_5O_{12}$/CNTs electrodes at different rates. The discharge capacities of bulk $Li_4Ti_5O_{12}$/CNTs decrease steeply with increasing discharge rates, whereas the nano-$Li_4Ti_5O_{12}$/CNTs decrease much slower at the same rate. It is noteworthy that the obtained capacity (112 mAh g^{-1}) of $Li_4Ti_5O_{12}$/CNTs nanocomposites at the 20 C is higher than that obtained at the 5 C (106.5 mAh g^{-1}) for the bulk $Li_4Ti_5O_{12}$/CNTs. This significantly improved rate capability of the nano-$Li_4Ti_5O_{12}$/CNTs electrode could be explained mainly by the reduced resistance and polarization of the electrode as described above. The nano-

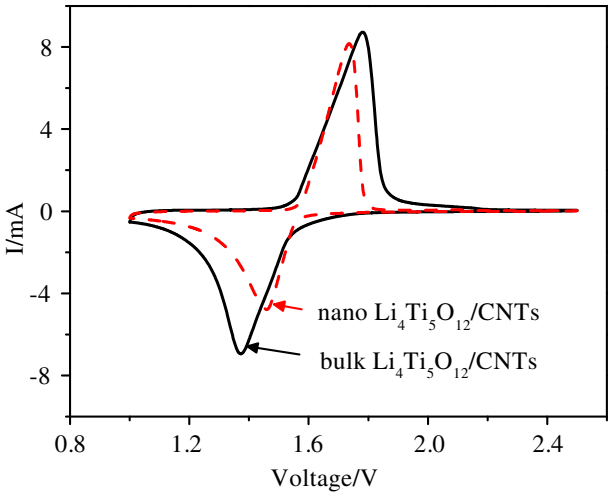

Fig. 5. Cyclic voltammograms of nano-$Li_4Ti_5O_{12}$/CNTs and bulk $Li_4Ti_5O_{12}$/CNTs electrodes at a scan rate of 1 mV s^{-1}.

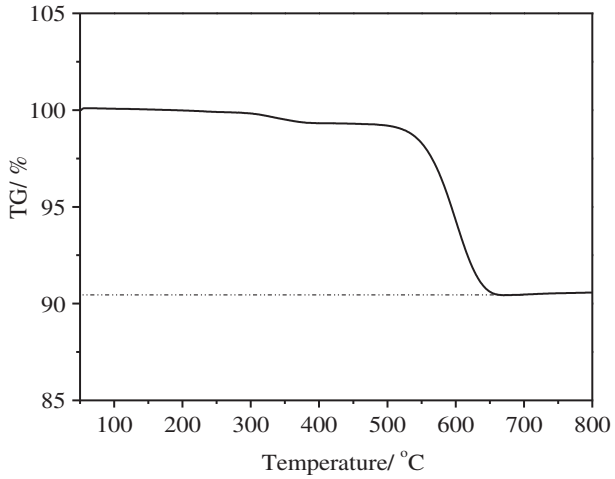

Fig. 4. TG curve of the nano-$Li_4Ti_5O_{12}$/CNTs composite synthesized by liquid phase deposition measured in air atmosphere.

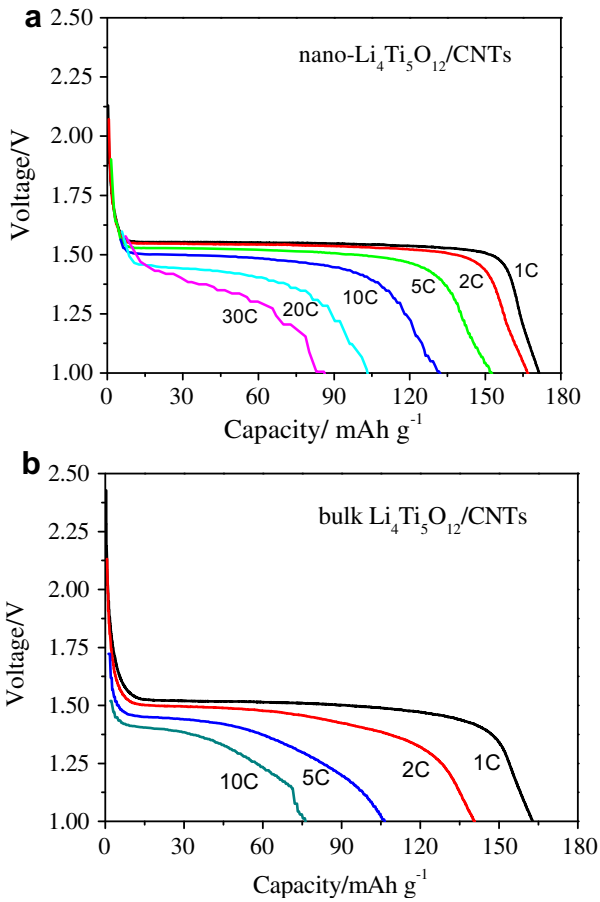

Fig. 6. Discharge curves of nano-$Li_4Ti_5O_{12}$/CNTs composite (a) and bulk $Li_4Ti_5O_{12}$/CNTs composites (b).

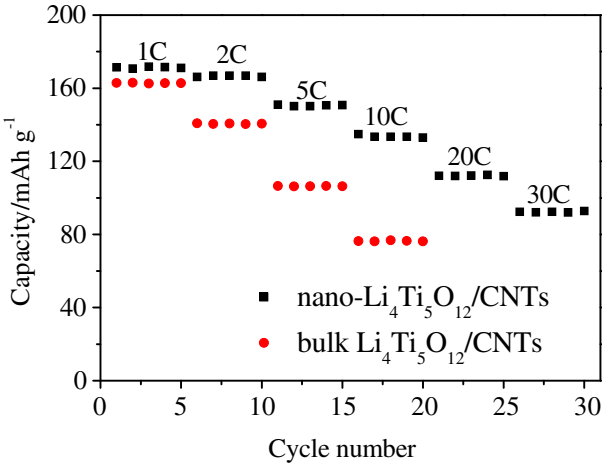

Fig. 7. Comparison of the rate capabilities of nano-$Li_4Ti_5O_{12}$/CNTs and bulk $Li_4Ti_5O_{12}$/CNT.

$Li_4Ti_5O_{12}$/CNTs composite also exhibited excellent cyclability with no noticeable decrease in performance over 100 cycles (Fig. 8). The discharge capacity loss was 0.5% at 1 C and 2% at 5 C. This result demonstrates that the structure of the nanocomposite is very stable, and the Li^+ ions insertion/extraction process is quite reversible even at high rates.

The superior rate capability and good cycling stability of the nano-$Li_4Ti_5O_{12}$/CNTs composites may be attributed to the following three aspects. Firstly, The CNTs work as a highly conductive matrix between $Li_4Ti_5O_{12}$ nanoparticles, which decreases the inner resistance of composite, therefore leading to enhanced Li storage properties. Secondly, the intimate interaction between the CNTs substrates and the $Li_4Ti_5O_{12}$ nanoparticles directly grown on them makes Li^+ ions effectively and rapidly conduct back and forth from the $Li_4Ti_5O_{12}$ nanoparticles to the current collector through the highly conducting CNTs network. Thirdly, uniform dispersion of the nanosized $Li_4Ti_5O_{12}$ particles growing on the CNTs matrices avoids aggregation, which is desired for cycle stability. Based on the above analyses, it is concluded that the synergetic effect between conducting CNTs and $Li_4Ti_5O_{12}$ nanoparticles is responsible for the excellent electrochemical performance of the overall electrode via the maximum utilization of electrochemically active CNTs and nanosized $Li_4Ti_5O_{12}$.

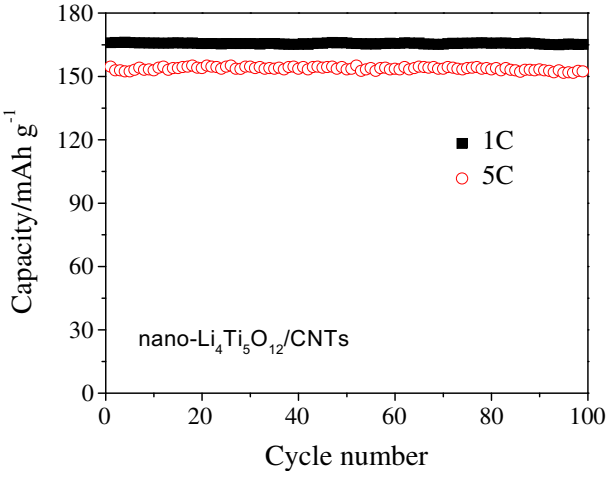

Fig. 8. Cycle performance curves of nano-$Li_4Ti_5O_{12}$/CNTs electrode at 1 °C and 5 C.

4. Conclusions

In summary, the $Li_4Ti_5O_{12}$/CNTs nanocomposite with excellent electrochemical properties has been successfully prepared through a facile liquid phase deposition. The $Li_4Ti_5O_{12}$ nanoparticles with a size of about 50 nm were homogeneously anchored on CNTs and effectively prevented the $Li_4Ti_5O_{12}$ nanoparticles from aggregating together. The $Li_4Ti_5O_{12}$/CNTs nanocomposite exhibited remarkable electrochemical property including highly reversible capacity, superior rate capability and good cycling stability, which makes it quite a suitable and promising anode material for high-performance lithium ion batteries.

Acknowledgements

This work was supported by the National Natural Science Foundation of China, Fundamental Research Funds for the Central Universities of China and the State Key Laboratory of New Ceramic and Fine Processing (Tsinghua University).

References

[1] K.M. Colbow, J.R. Dahn, R.R. Haering, J. Power Sources 26 (1989) 397–402.
[2] T. Ohzuku, Y. Iwakoshi, K. Sawai, J. Electrochem. Soc. 140 (1993) 2490–2498.
[3] A. Guerfi, S. Sevigny, M. Lagace, P. Hovington, K. Kinoshita, K. Zaghib, J. Power Sources 88 (2003) 88–94.
[4] R. Li, Z.L. Tang, Z.T. Zhang, Electrochem. Commun. 7 (2005) 894–899.
[5] T. Ohzuku, A. Ueda, N. Yamamoto, J. Electrochem. Soc. 142 (1995) 1431–1435.
[6] L. Cheng, J. Yan, G.N. Zhu, J.Y. Luo, C.X. Wang, Y.Y. Xia, J. Mater. Chem. 20 (2010) 595–602.
[7] E.M. Sorensen, S.J. Barry, H.K. Jung, J.R. Rondinelli, J.T. Vaughey, K.R. Poeppelmeier, Chem. Mater. 18 (2006) 482–489.
[8] K. Zaghib, M. Armand, M. Gauthier, J. Electrochem. Soc. 145 (1998) 3135–3140.
[9] K.S. Park, A. Benayad, D.J. Kang, S.G. Doo, J. Am. Chem. Soc. 130 (2008) 14930–14931.
[10] T. Doi, Y. Miwa, Y. Iriyama, T. Abe, Z. Ogumi, J. Phys. Chem. C 113 (2009) 7719–7722.
[11] S. Scharner, W. Weppner, P. Schmid-Beurmann, J. Electrochem. Soc. 146 (1999) 857–861.
[12] A.S. Arico, P. Bruce, B. Scrosati, J.M. Tarascon, W. Van Schalkwijk, Nat. Mater. 4 (2005) 366–377.
[13] A.S. Prakash, P. Manikandan, K. Ramesha, M. Sathiya, J.M. Tarascon, A.K. Shukla, Chem. Mater. 22 (2010) 2857–2863.
[14] J. Gao, J.R. Ying, C.Y. Jiang, C.R. Wan, J. Power Sources 166 (2007) 255–259.
[15] G.J. Wang, J. Gao, L.J. Fu, N.H. Zhao, Y.P. Wu, T. Takamura, J. Power Sources 174 (2007) 1109–1112.
[16] L. Shen, C. Yuan, H. Luo, X. Zhang, L. Chen, H. Li, J. Mater. Chem. 22 (2011) 14414–14416.
[17] J.P. Zhu, J.J. Zhao, H.W. Yang, G. Yang, Adv. Sci. Lett. 4 (2011) 484–487.
[18] A.D. Robertson, L. Trevino, H. Tukamoto, J.T.S. Irvine, J. Power Sources 81-82 (1999) 352–357.
[19] Z. Zhong, Electrochem. Solid-State Lett. 10 (2007) A267–A269.
[20] J. Wolfenstine, J.L. Allen, J. Power Sources 180 (2008) 582–585.
[21] M.S. Park, S.A. Needham, G.X. Wang, Y.M. Kang, J.S. Park, S.X. Dou, H.K. Liu, Chem. Mater. 19 (2007) 2406–2410.
[22] I. Moriguchi, Y. Shono, H. Yamada, T. Kudo, J. Phys. Chem. B 112 (2008) 14560–14565.
[23] Z.H. Wen, Q. Wang, Q. Zhang, J.H. Li, Adv. Funct. Mater. 16 (2006) 2141–2146.
[24] A.L.M. Reddy, M.M. Shaijumon, S.R. Gowda, P.M. Ajayan, Nano Lett. 9 (2009) 1002–1006.
[25] B. Gao, C.Z. Yuan, L.H. Su, L. Chen, X.G. Zhang, J. Solid State Electrochem. 13 (2009) 1251–1257.
[26] Y. Hou, Y.W. Cheng, T. Hobson, J. Liu, Nano Lett. 10 (2010) 2727–2733.
[27] Y. He, L. Huang, J.S. Cai, X.M. Zheng, S.G. Sun, Electrochim. Acta 55 (2010) 1140–1144.
[28] B. Liu, H.C. Zeng, Chem. Mater. 20 (2008) 2711–2788.
[29] Y.G. Guo, J.S. Hu, L.J. Wan, Adv. Mater. 20 (2008) 2878–2887.
[30] C.H. Jiang, E. Hosono, H.S. Zhou, Nano Today 1 (2006) 28–33.
[31] I. Moriguchi, R. Hidaka, H. Yamada, T. Kudo, H. Murakami, N. Nakashima, Adv. Mater. 18 (2006) 69–73.
[32] Y.D. Yang, L.T. Qu, L.M. Dai, T.S. Kang, M. Durstock, Adv. Mater. 19 (2007) 1239–1243.
[33] X. Lu, T. Imae, J. Phys. Chem. C 111 (2007) 2416–2420.
[34] H.T. Yu, X. Quan, S. Chen, H.M. Zhao, J. Phys. Chem. C 111 (2007) 12987–12991.
[35] Y.R. Jhan, J.G. Duh, J. Power Sources 198 (2012) 294–297.
[36] J. Huang, Z. Jiang, Electrochim. Acta 53 (2008) 7756–7759.
[37] Y. Shi, L. Wen, F. Li, H.M. Chen, J. Power Sources 196 (2011) 8610–8617.